



# Inhibitor of glutamine metabolism V9302 promotes ROS-induced autophagic degradation of B7H3 to enhance antitumor immunity

Received for publication, August 12, 2021, and in revised form, February 7, 2022. Published, Papers in Press, February 19, 2022.

<https://doi.org/10.1016/j.jbc.2022.101753>

Qian Li<sup>1,2,‡</sup>, Xiaofang Zhong<sup>1,2,‡</sup>, Weicheng Yao<sup>3,‡</sup>, Junli Yu<sup>1,2</sup>, Chao Wang<sup>1,4</sup>, Zongyan Li<sup>1,5</sup> , Shengqing Lai<sup>1,2</sup>, Fanli Qu<sup>1,2</sup>, Xiaoyan Fu<sup>1,2</sup>, Xiaojia Huang<sup>1,2</sup>, Dawei Zhang<sup>1,5,\*</sup>, Yujie Liu<sup>3,6,\*</sup>, and Haiyan Li<sup>1,2,\*</sup> 

From the <sup>1</sup>Guangdong Provincial Key Laboratory of Colorectal and Pelvic Floor Diseases, The Sixth Affiliated Hospital, Sun Yat-sen University, Guangzhou, China; <sup>2</sup>Department of Breast Surgery, The Sixth Affiliated Hospital of Sun Yat-sen University, Guangzhou, China; <sup>3</sup>Guangdong Provincial Key Laboratory of Malignant Tumor Epigenetics and Gene Regulation, Medical Research Center, Sun Yat-sen Memorial Hospital, Sun Yat-sen University, Guangzhou, China; <sup>4</sup>Department of Pathology, and <sup>5</sup>Department of Hepatobiliary Surgery, The Sixth Affiliated Hospital of Sun Yat-sen University, Guangzhou, China; <sup>6</sup>Breast Tumor Center, Sun Yat-sen Memorial Hospital, Sun Yat-sen University, Guangzhou, China

Edited by Eric Fearon

Despite the enormous successes of anti-PD-1/PD-L1 immunotherapy in multiple other cancer types, the overall response rates of breast cancer remain suboptimal. Therefore, exploring additional immune checkpoint molecules for potential cancer treatment is crucial. B7H3, a T-cell coinhibitory molecule, is specifically overexpressed in breast cancer compared with normal breast tissue and benign lesions, making it an attractive therapeutic target. However, the mechanism by which B7H3 contributes to the cancer phenotype is unclear. Here we show that the expression of B7H3 is negatively related to the number of CD8<sup>+</sup> T cells in breast tumor sites. In addition, analysis of the differentially expressed B7H3 reveals that it is inversely correlated to autophagic flux both in breast cancer cell lines and clinical tumor tissues. Furthermore, block of autophagy by bafilomycin A1 (Baf A1) increases B7H3 levels and attenuates CD8<sup>+</sup> T cell activation, while promotion of autophagy by V9302, a small-molecule inhibitor of glutamine metabolism, decreases B7H3 expression and enhances granzyme B (GzB) production of CD8<sup>+</sup> T cells *via* regulation of reactive oxygen species (ROS) accumulation. We demonstrate that combined treatment with V9302 and anti-PD-1 monoclonal antibody (mAb) enhances antitumor immunity in syngeneic mouse models. Collectively, our findings unveil the beneficial effect of V9302 in boosting antitumor immune response in breast cancer and illustrate that anti-PD-1 together with V9302 treatment may provide synergistic effects in the treatment of patients insensitive to anti-PD-1 therapy.

Breast cancer is reported as the most commonly diagnosed cancer and the leading cause of cancer death in women based on Global Cancer Statistics 2020 (1). Patients' survival was dramatically improved over the past 10 years, as available

treatment modalities optimized, including surgery, radiotherapy, chemotherapy, endocrine therapy, targeted biological therapy, and immunotherapy. With the clinical success of immune checkpoint inhibitors in some cancer types, immunotherapy has now undergone a paradigm transition from "immune enhancement" strategy to "immune normalization" strategy. The enhancement strategy focuses on enhancing antitumor immune response by using IL-2, interferons (IFNs), and CAR-T cells. Normalization treatment strategy suggests removing tumor-induced immune-inhibitory molecules that inhibit antitumor immunity including PD-1, PD-L1, CTLA-4, etc. Despite immunotherapy, employing anti-PD-1/PD-L1 has been widely utilized in multiple malignant tumors (2), clinical trials evaluating monotherapy of anti-PD-1/PD-L1 for patients with early-phase breast cancer showed marginal effect with the objective response rate (ORR) ranging from 5.2 to 18.5% (3–6). Though the following trials adding the anti-PD-1/PD-L1 mAb to chemotherapy demonstrated improved response rate among a small subset of triple-negative breast cancer (TNBC) patients (7, 8), JAVELIN (3) showed ORR was only 2.8%, and Keynote028 (6) resulted in an ORR of 12.0% in estrogen receptor positive (ER<sup>+</sup>) breast cancer patients, indicating the poor immunogenic nature of breast cancer and less responsive to PD-1/PD-L1 blockade. It was probably due to the lower tumor mutation burden (TMB) to generate immunogenic neoantigens, decreased tumor-infiltration lymphocytes (TILs) content, weak PD-1/PD-L1 level, infiltration of immunosuppressive cells such as myeloid-derived suppressor cells (MDSCs), regulatory T cells (Treg), and so on (9, 10), and upregulation of other inhibitory immune checkpoints such as B7H3, VISTA, TIM-3, CD73, CTLA-4, LAG-3, etc (11).

CD276, also known as B7 homolog 3 (B7H3), is a cell surface glycoprotein antigen, which is highly expressed in lung, breast, ovarian, renal, and colon cancers, but not in normal tissues. Additionally, B7H3 was related to advanced tumor grade and poor prognosis in multiple cancer types and implicated in tumor proliferation, migration, invasion,

<sup>‡</sup> These authors contributed equally to this work.

\* For correspondence: Haiyan Li, [lihy27@mail.sysu.edu.cn](mailto:lihy27@mail.sysu.edu.cn); Yujie Liu, [liuyujie554@163.com](mailto:liuyujie554@163.com); Dawei Zhang, [zhangdaweiwinner@163.com](mailto:zhangdaweiwinner@163.com).

## V9302 promotes B7H3 degradation to enhance anti-tumor immunity

angiogenesis, and chemo-resistance (12–15). In addition to these protumoral activities, B7H3 is being given an increasing amount of attention because of its immune-regulatory functions. It was initially reported as an immune stimulatory molecule and now is believed to act as an immune checkpoint ligand contributing to immune evasion (16). It was reported that B7H3 blockade or deficiency augmented intratumoral CD8<sup>+</sup> T-cells infiltration and suppressed tumor growth. Combining anti-B7H3 with PD-1 blockade showed a much better antitumoral effect than monotherapy (17). Therefore, B7H3 is considered as a promising alternative tumor immunotherapy target, especially for patients insensitive to anti-PD-1/PD-L1 therapy.

Increased glutamine (Gln) uptake is a common hallmark of many types of cancer such as breast, lung, and colorectal cancer (18) and is identified to link to patients' poor survival in breast cancer (19, 20). It provides carbon and nitrogen to support anabolic metabolism and is the "fuel" for the tricarboxylic acid cycle (TCA) in both tumor cell (21) and T cell (22). Blocking Gln metabolism results in dual effects that it inhibits tumor cell growth, but strengthens immune response by directly promoting T-cells proliferation and maintaining its activation (22, 23). In addition, Gln-blocking regulates immune checkpoints such as PD-L1 expression on tumor cells *via* activating NK- $\kappa$ B or EGFR/ERK/c-Jun signaling pathways (24, 25). These make modulation of glutamine metabolism a meaningful antitumor strategy. V9302 is a selective and potent small-molecule antagonist of amino acid transporter ASCT2 (SLC1A5). Previous studies identified that V9302 exhibited a better antitumor potency than the other Gln metabolism inhibitors, GPNA and CB-839 (26). However, whether V9302 can inhibit breast cancer progression and sensitize low immunogenic breast cancer to immunotherapy is still an open question. Since B7H3 is highly expressed in breast cancer tissues, we studied the relationship between B7H3 expression and CD8<sup>+</sup> T-cell activation and infiltration in the breast tumor microenvironment (TME). Furthermore, we investigated the role of Gln metabolism antagonist V9302 in decreasing B7H3 expression and its function in restoration of antitumor immune response in combination with anti-PD-1 mAb.

### Results

#### **Identification of the relationship between autophagosome formation, B7H3 expression and CD8<sup>+</sup> T-cells infiltration in breast cancer**

To identify if B7H3 expression affects the immune environment of breast cancer, we first quantified CD8<sup>+</sup>T cells and T effector memory (Tem) cells in each breast cancer tissue from Curtis database by estimating gene expression data using xCell algorithm. Patients were stratified by ER status into ER<sup>+</sup> and ER<sup>-</sup> subgroups. The composition of CD8<sup>+</sup> T cells infiltration was negatively related to the expression of B7H3 mRNA in both subgroups. The same trend was also observed in Tem cells (Fig. S1, A and B). These results inspired us to further investigate the relationship between B7H3 and CD8<sup>+</sup> T-cells content in tumor tissues of patients from our clinical

core. The clinicopathological status of patients with breast cancer is described in detail in Table S1. Immunohistochemistry (IHC) images showed CD8 positive cell number was higher in low B7H3 expression subgroup divided by the cutoff value of median B7H3 IHC score and vice versa ( $p = 0.002$ ) (Fig. 1, A, B, and D). The analysis of the online public dataset together with data from our clinical core both suggested B7H3 might influence the content of CD8<sup>+</sup> T cells in breast tumor sites. To clarify the potential mechanism contributing to differential expression of B7H3, we found that B7H3 level was inversely related to the formation of autophagosome as marked by LC3-II dots. We divided patients into LC3-dots<sup>more</sup> and LC3-dots<sup>less</sup> subgroups by the median number of LC3-II dots, and tumor tissues in LC3-dots<sup>more</sup> subgroup had a lower level of B7H3 expression ( $p = 0.026$ ) (Fig. 1, B, C, and E). Based on these observations, we assumed B7H3 expression regulated by autophagy pathway participated in immune cells infiltration in breast cancer.

#### **B7H3 is mainly degraded by the autophagy-lysosomal pathway**

Autophagy is an evolutionarily conserved cellular recycling process, which involves the sequestration of target proteins and organelles in autophagosomes and subsequent delivery of the cargo to lysosomes for degradation. Lipidated LC3, also known as LC3-II, is a molecular marker of the autophagosome, which is essential for autophagosome formation and p62 recruitment to the autophagosomes. After interacting with LC3-II, p62 links cargos to the autophagic machinery to enable their degradation in the lysosome (27). We observed human breast cancer cell lines expressed different levels of LC3-II and B7H3 protein. Interestingly, we found that BT-474 expressed less total B7H3, while stained higher autophagy marker protein LC3-II compared with MCF-7 and T47D in ER<sup>+</sup> breast cancer cell lines. Similarly, MDA-MB-231 expressed less B7H3 and more LC3-II than BT-549 in ER<sup>-</sup> breast cancer cell lines (Fig. 2A). Gene expression pattern of B7H3 and LC3-II was consistent with the result from IHC staining of clinical sections (Fig. 1, B and C), suggesting that B7H3 expression was negatively related to the level of autophagy. Furthermore, we detected the localization of B7H3 in breast cancer cells and found besides expressing on the cell membrane as B7H3 is a transmembrane protein, it also exhibited a punctate cytoplasmic distribution colocalized with autophagosomes and lysosomes marked by LC3-II and LAMP1, respectively (Fig. 2B). Next, we investigated if B7H3 degraded *via* autophagy pathway. Because the steady-state levels of autophagosomes reflect the difference in the amount of LC3-II generation and degradation, Baf A1 is usually used to demonstrate the total LC3-II synthesis by inhibiting autolysosome acidification and autophagosome-lysosome fusion. We found that application of autophagy inhibitor Baf A1 resulted in the accumulation of LC3-II and B7H3 proteins and increase of B7H3<sup>+</sup>-cell abundance in MCF-7 and BT-474 cells (Fig. 2, C and D), indicating B7H3 was actively routed to the lysosome for degradation. Since B7H3 has been reported to be associated with reduced T-cell activation and low density of

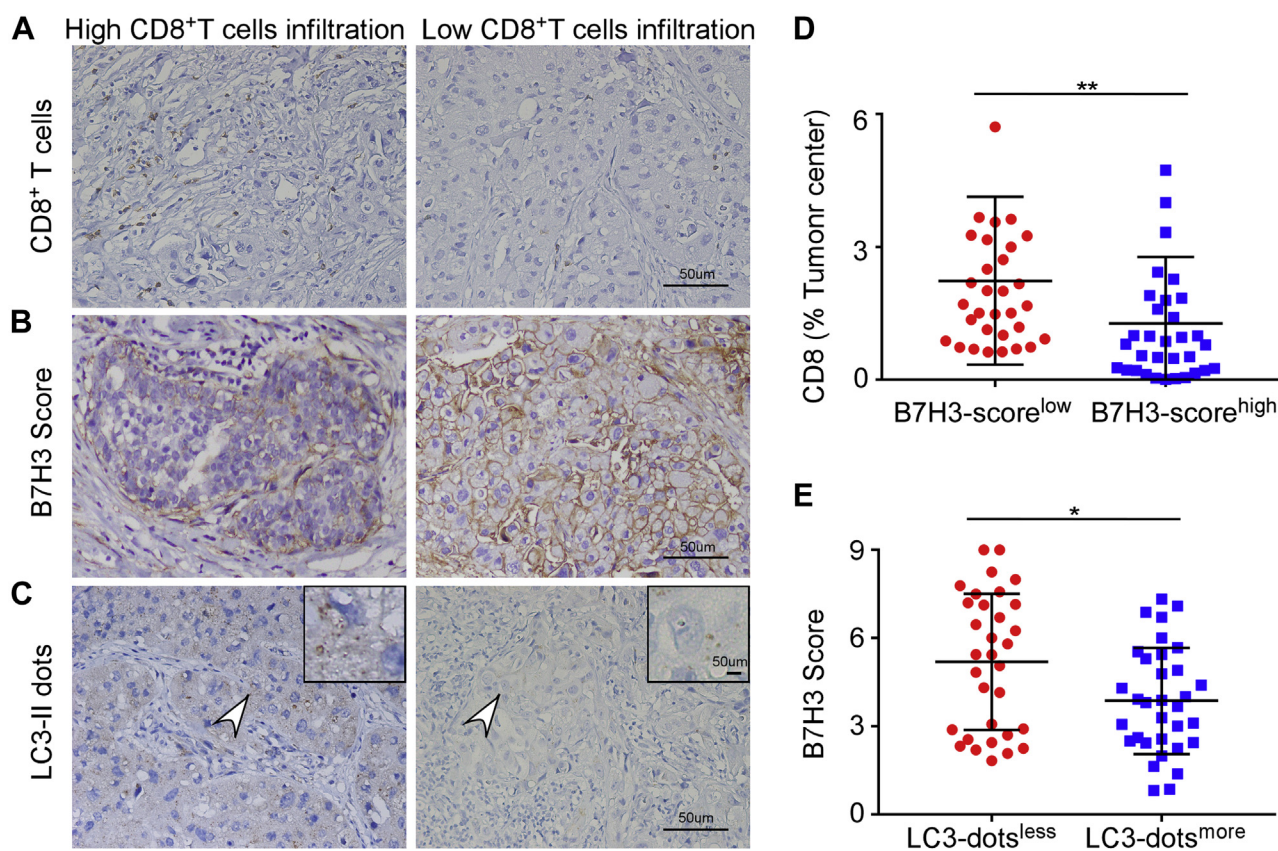


**Figure 1. Autophagy, B7H3 expression, and CD8<sup>+</sup> T cells infiltration profile in breast cancer.** Representative images of CD8<sup>+</sup> T cell infiltrated areas (A), B7H3 expression (B) and LC3-II dots (C) by IHC in breast cancer tissue. Scale bar, 50  $\mu$ m. D, the relationship between B7H3 expression and CD8<sup>+</sup> T cell infiltration percentage. E, the relationship between autophagy and B7H3 expression. Tumor samples were obtained from 65 patients with invasive breast carcinoma at the Sixth Affiliated Hospital, and data were presented as means  $\pm$  SD; \* $p$  < 0.05 by Mann-Whitney U test. B7H3, B7 homolog 3; IHC, immunohistochemistry.

TILs in TME, we examined whether Baf A1 treatment mitigated the cytotoxic T lymphocytes (CTLs)-mediated antitumor reaction by using flow cytometer. The results showed CD8<sup>+</sup> T cells primed by Baf A1 treated MCF-7 or BT474 cell lysate-pulsed dendritic cells (DCs) markedly decreased granzyme B (GzB) production and CD69 expression than that primed by untreated cells lysate-pulsed DCs (Fig. 2, E and F). Collectively, these data suggested that B7H3 was degraded by the autophagy-lysosomal degradation pathway in breast cancer cells, and block of autophagy inhibited CD8<sup>+</sup> T-cell activation.

#### V9302 controls B7H3 expression via increased autophagy

V9302 was reported to decrease cell growth, increase cell apoptosis, promote reactive oxygen species (ROS) generation, and modulate autophagy in multiple types of cancer cells (26). We therefore investigated whether V9302-induced autophagy controls B7H3 expression and the following antitumor immune response. Consistent with previous studies, we also found that V9302 inhibited MCF-7 and BT-474 cell viability (Figs. 3, A and B and S2, A and B) and cell proliferation (Figs. 3C and S2C) in a concentration and time-dependent manner, with the inhibitory rate around 30% and 40%, respectively, at the concentration of 2  $\mu$ g/ml. In addition, V9302-promoted cell apoptotic with the percentage of apoptosis cells increased about tenfold at the

concentration of 2  $\mu$ g/ml when comparing with control cells (Figs. 3D and S2D), and cleaved caspase-3 (only detected in BT-474 cells) and PARP (detected in both cell lines) was elevated with increasing concentration of V9302 (Figs. 3E and S2E). In addition, V9302 exposure in MCF-7 and BT-474 cells led to a significantly increased level of intracellular ROS (Figs. 3F and S2F). Cancer cells deprived of nutrition supply by glutamine metabolism inhibitor tend to initiate autophagy to maintain tumor survival, and accumulated ROS can also induce autophagy. We then examined V9302-triggered autophagy in breast cancer cells. Western blot revealed that the LC3-II level was elevated in MCF-7 cells treated with V9302 (Fig. 3G), with the accompanied reduction of B7H3 expression and B7H3-positive cells abundance in a concentration-dependent manner (Fig. 3, G and H). Similar results were also observed in BT-474 (Fig. S2, G and H). However, application of Baf A1 inhibited V9302-induced B7H3 degradation (Fig. S3A). To exclude V9302-reduced B7H3 expression by transcriptional regulation or other protein degradation mechanisms, we assessed mRNA expression of B7H3 by qPCR in the presence of V9302 and found that V9302 had little effects on B7H3 mRNA expression (Fig. S3B). The proteasome inhibitor MG132 promotes accumulation of target proteins, which are degraded *via* the ubiquitin-proteasome pathway. Next, we

## V9302 promotes B7H3 degradation to enhance anti-tumor immunity

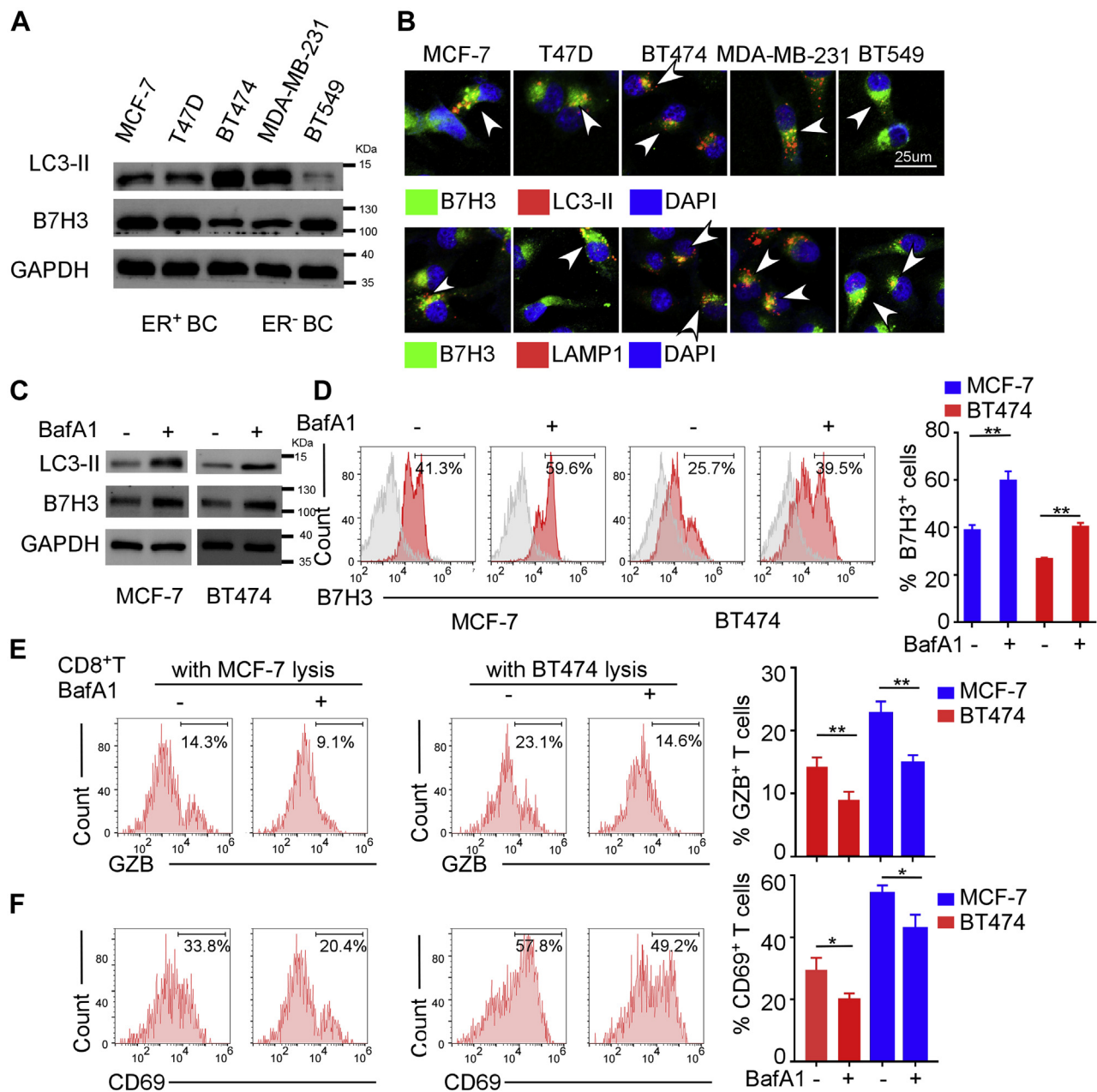


**Figure 2. The degradation of B7H3 mainly depends on the autophagy-lysosomal pathway.** *A*, Western blot showing LC3-II, a marker of autophagy, and B7H3 expression in different breast cancer cell lines. *B*, immunofluorescence detection of LC3-II/LAMP1 and B7H3 in different breast cancer cell lines which showing B7H3 was enriched within autophagosomes and lysosomes. Scale bar, 25 µm. *C*, Western blot showing LC3-II and B7H3 expression in MCF-7 and BT-474 treated with or without 150 nM Baf A1 for 6 h, an inhibitor of lysosome. *D*, flow cytometry analysis showing B7H3 expression in MCF-7 and BT-474 treated with or without Baf A1. *E* and *F*, flow cytometry analysis showing the proportion of Granzyme B (GZB)<sup>+</sup>CD8<sup>+</sup>T cells (*E*) and CD69<sup>+</sup>CD8<sup>+</sup>T cells (*F*). The *left* showed the representative flow cytometry images, and *right* showed the statistical columns. All experiments were performed three times independently. For *D–F*, data were presented as means ± SD, \**p* < 0.05, \*\**p* < 0.01 by Student's *t* test. B7H3, B7 homolog 3.

blocked the proteolytic activity by using MG132 and observed that the protein level of B7H3 was significantly enhanced, indicating that partially B7H3 protein degrades *via* proteasome pathway. However, MG132 didn't restore B7H3 expression when treated with V9302 (Fig. S3C), indicating that V9302 induced degradation of B7H3 mainly through autophagy pathway but not proteasome pathway.

Furthermore, we investigated whether decreased B7H3 exerted by V9302 treatment could also influence the

functions of CTLs that were generated by incubating CD8<sup>+</sup> T cells with mature DCs pulsed with tumor lysates. We observed that V9302 exposure enhanced the production of GzB and CD69 expression of CTLs in both MCF-7 and BT-474 models (Figs. 3, *I* and *J* and S2, *I* and *J*). Collectively, these results suggested that V9302 not only influenced cell proliferation and apoptosis, but also enhanced antitumor immunity by downregulating B7H3 expression *via* increased autophagy.

## V9302 promotes B7H3 degradation to enhance anti-tumor immunity

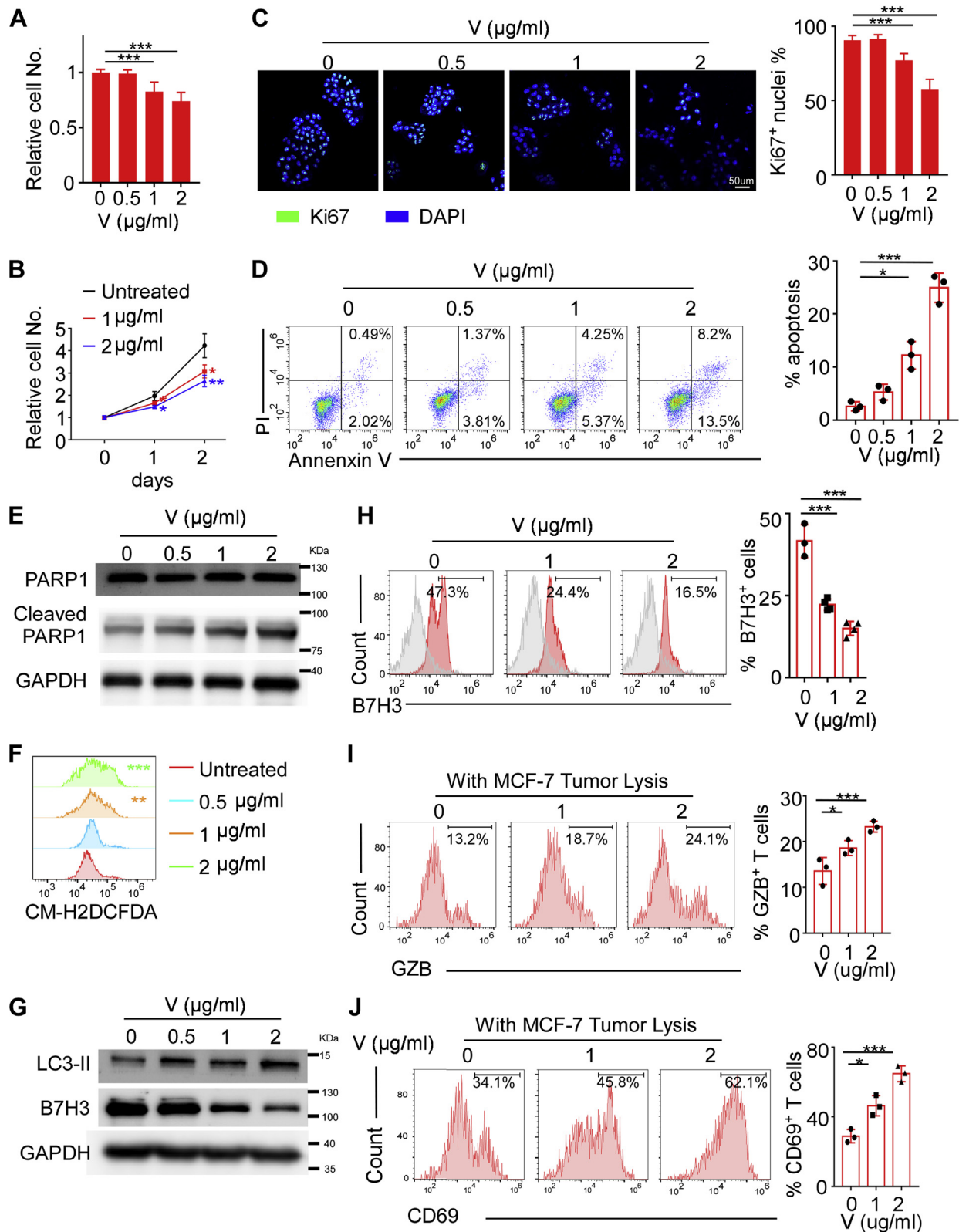


**Figure 3. V9302 promotes B7H3 degradation via increased ROS-autophagy axis in MCF-7.** A and B, cell viability assay (trypan blue exclusion assay) showing the effect of different concentration and treatment time of V9302 (V) on MCF-7. C, Ki67 staining showing the cell proliferation with different concentration of V9302 (V). Scale bar, 50 μm. D, apoptosis assay by annexin V-FITC/PI staining showing the percentages of apoptotic cells when treated with different concentration of V9302 (V). E, the expression of cleaved/total PARP in MCF-7 cells cultured with different concentration of V9302 (V). F, flow cytometry assay probed by DCFDA showing ROS generation in the treatment of different concentration of V9302 (V). G, Western blot showing LC3-II and B7H3 expression in MCF-7 treated with different concentration of V9302 (V). H, flow cytometry analysis showing B7H3 expression on MCF-7 with different concentration of V9302 (V). I and J, flow cytometry analysis showing the proportion of Granzyme B (GZB)<sup>+</sup>CD8<sup>+</sup>T cells (I) and CD69<sup>+</sup>CD8<sup>+</sup>T cells (J). For A–C, n = 5 independent experiments, for H, n = 4 independent experiments, for the rest, n = 3 independent experiments. Data were presented as means ± SD. \*p < 0.05; \*\*\*p < 0.001 by Student's t test. B7H3, B7 homolog 3; ROS, reactive oxygen species.

## V9302 promotes B7H3 degradation to enhance anti-tumor immunity

### *N*-acetylcysteine (NAC) rescues V9302-induced autophagy and B7H3 degradation

ROS is a key regulatory factor of autophagy in various types of cancers, which induces autophagy by regulating mTOR, MAPK signaling, and p53 pathway (28). Moreover, Gln deficiency was reported to activate ROS by JAK2/STAT3 pathway (29). To determine whether V9302-regulated autophagy was due to excessive ROS accumulation, we used NAC, which can easily penetrate the cell membrane directly to neutralize ROS. We found that ROS neutralization reversed V9302-induced cell viability and proliferation decrease, apoptosis, and ROS production (Fig. 4, A–E). In addition, ROS blockade with NAC prevented V9302-induced LC3-II synthesis, B7H3 degradation and restored B7H3-positive cells percentage (Fig. 4, F and G).

To probe V9302-enhanced CD8<sup>+</sup> CTLs activation through regulating ROS-autophagy-B7H3 axis, we collected cell lysate from MCF-7 by 5 to 6 freeze–thaw cycles after exposure to 0, 1, and 2 μg/ml V9302 with or without NAC. Then, we activated CD8<sup>+</sup>T cells with DCs stimulated by differently treated cell lysate and found that NAC decreased GzB and CD69 expression on CD8<sup>+</sup> CTLs (Fig. 4, H and I). Collectively, these results suggested that ROS neutralization not only influences the cell proliferation and death regulated by V9302, but also diminished antitumor immunity promoted by V9302 *via* ROS-autophagy-B7H3 pathway.

### V9302 sensitizes breast cancer to PD-1 blockade

Despite the enormous successes of anti-PD-1/PD-L1 immunotherapy in multiple cancers, the overall response rates of breast cancer remain suboptimal. Blockade of B7H3 was reported to exert potent therapeutic effects and can sensitize anti-PD-1 therapy in multiple mouse tumor models. To probe if V9302 might sensitize breast cancer to PD-1 antibody, we orthotopically implanted EO771 and 4T1 mammary breast tumor cells into mice fat pad to establish syngeneic murine models. It was reported that EO771 tumors are ER weakly positive (Fig. S4) (30–32) and 4T1 tumors are highly immunosuppressive (33). Experimental mice were divided into four groups, receiving IgG (10 mg/kg ip.), anti-PD-1 antibody (10 mg/kg ip.), V9302 (75 mg/kg ip.), or anti-PD-1 antibody plus V9302 for 2 weeks, respectively. Anti-PD-1 alone exhibited no antitumoral activity in EO771 syngeneic model, while it slightly suppressed tumor growth in 4T1 model. V9302 fractionally limited tumor growth as a single agent in both mouse models. Interestingly, it was noticed that the combination of anti-PD-1 antibody and V9302 significantly inhibited tumor growth, especially in EO771 mouse model (Figs. 5, A–C and S5, A–C). Additionally, immunofluorescent staining demonstrated that V9302 plus anti-PD-1 therapy resulted in remarkably enhanced apoptosis of tumor cells denoted as Tunel<sup>+</sup> cells in the tumor grafts than that of anti-PD-1 or V9302 monotherapy tumor tissues (Figs. 5D and S5D). These results demonstrated that V9302 sensitized breast cancer to anti-PD-1 therapy.

### V9302 downregulated B7H3 expression and increased CD8<sup>+</sup>T cells infiltration in the tumors in vivo

To investigate the mechanisms of V9302-sensitized breast cancer to anti-PD-1, we collected EO771 and 4T1 allografts

treated as described above. As our *in vitro* experiments had proved that V9302 employment downregulates B7H3 level *via* modulating autophagy, and therefore enhancing antitumor immunity, we first detected autophagic flux by immunofluorescence immunostaining. The results revealed that anti-PD-1 had little effect on autophagosome formation, while V9302 promoted autophagy as a single agent. Anti-PD-1 combined with V9302 showed no more LC3-II marked autophagosome than V9302 alone in EO771 model (Fig. 6A). Similar results were observed in 4T1 tumors, except for anti-PD-1, which had a faintly inhibitory effect on autophagosome formation (Fig. S6A). Next, we assessed surface B7H3 levels by flow cytometry and total B7H3 expression by immunofluorescence and observed that V9302 decreased surface and total B7H3 expression in both mice models, while anti-PD-1 mildly increased surface B7H3 expression. When combined with V9302, anti-PD-1-triggered B7H3 upregulation was abolished (Figs. 6, B and C and S6, B and C).

Previous studies indicated that majority of breast cancer patients did not benefit from anti-PD-1/PD-L1 therapy, which might be associated with a low level of TILs or CD8<sup>+</sup> T-cells infiltration (34–37). We therefore detect whether the synergy of V9302 and anti-PD-1 was related to increased CD8<sup>+</sup> T-cells infiltration assayed by immunofluorescence and flow cytometry and whether degradation of B7H3 replenished the immune environment. The results showed that anti-PD-1 antibody had a limited effect on CD8<sup>+</sup> T-cells infiltration, while V9302 remarkably increased CD8<sup>+</sup> T cells content in tumor tissues. When combining V9302 with anti-PD-1 mAb, the infiltrated CD8<sup>+</sup> T-cell number was even double that in V9302 monotherapy group (Figs. 6, D and E and S6, D and E). Furthermore, V9302 exposure showed a prominent GzB<sup>+</sup> CD8<sup>+</sup> T-cells infiltration in tumors, and the proportion of GzB<sup>+</sup> CD8<sup>+</sup> T cells was further significantly increased when V9302 combined with anti-PD-1. Nevertheless, the percentage of GzB<sup>+</sup> CD8<sup>+</sup> T cells was only mildly increased in EO771 model, while unchanged in 4T1 model with anti-PD-1 as a single agent (Figs. 6F and S6F). Collectively, these *in vivo* results confirmed that V9302 promoted autophagy to induce B7H3 degradation, which in turn relieved the suppressive immune-environment, strengthened CD8<sup>+</sup> T-cells infiltration and activation, and thus sensitized breast cancer to PD-1 blockade therapy.

## Discussion

Cancer cells need specific metabolic programs to support their prodigious energy requirements and ever-increasing biosynthesis to generate the building blocks required for rapid cell division. Metabolic reprogramming is now a known hallmark of cancers with two striking and broadly conserved characteristics: increased glucose and amino acid glutamine consumption (38). Aerobic glycolysis, also called Warburg effect, where cancer cells uptake extremely high levels of glucose and transform them into lactate and adenosine 5'-triphosphate (ATP) to meet the energetic requirements of cancerous cells, even in the presence of adequate oxygen. However, enhanced glycolysis alone is insufficient to satisfy the

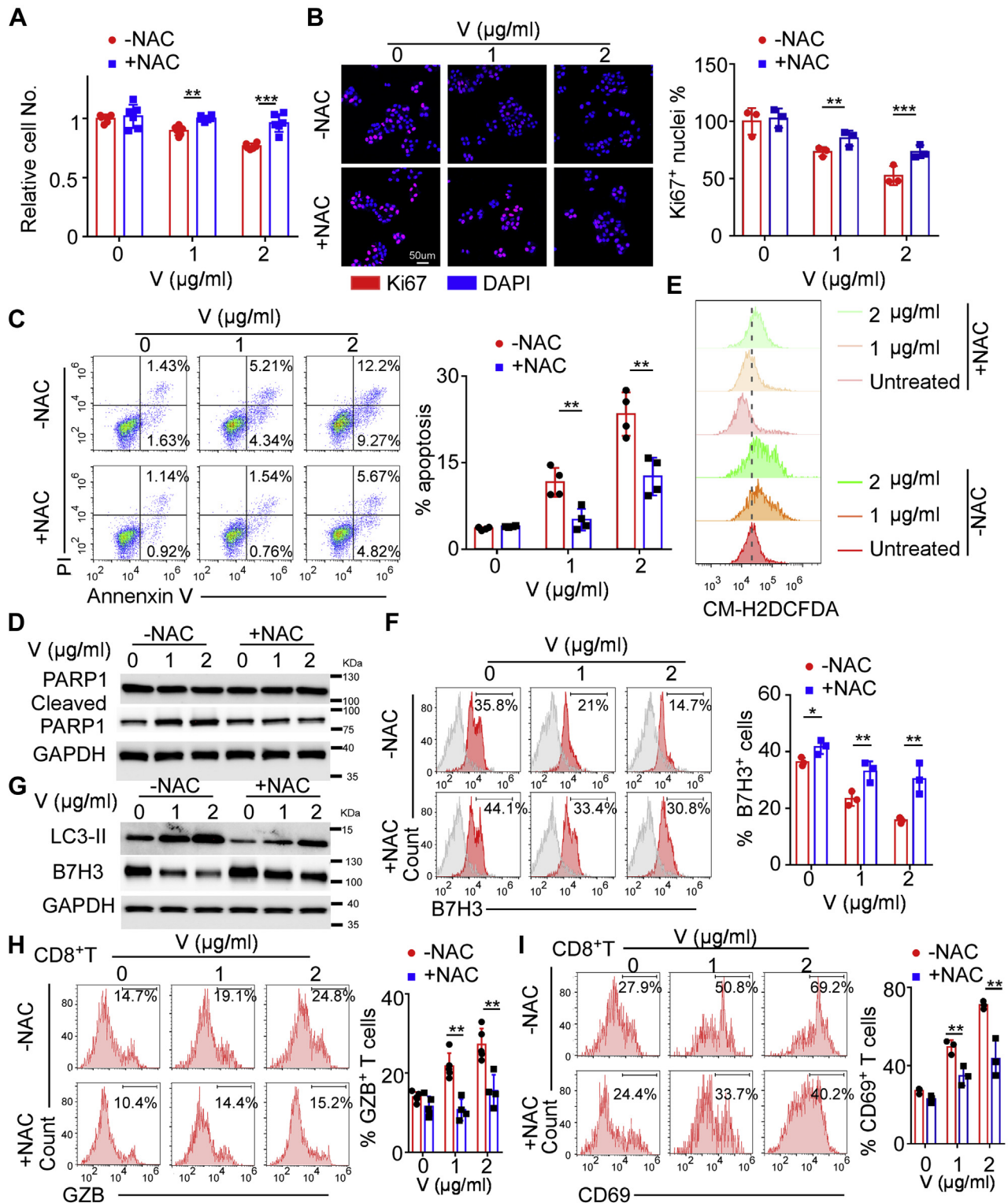


**Figure 4. NAC blocks V9302 modulated ROS- autophagy-B7H3 axis in MCF-7.** A, cell viability assay showing 5 mM NAC reversed the inhibitory effects of different concentration of V9302 (V). B, Ki67 staining showing 5 mM NAC restores cell proliferation inhibited by different concentration of V9302 (V). C, apoptosis assay by annexin V-FITC/PI staining showing 5 mM NAC decreased the percentages of apoptotic cells when treated with different concentration of V9302 (V). D, the apoptosis of MCF-7 cells was determined by Western blotting for cleaved and total PARP with different dose of V9302 (V) with or without 5 mM NAC treatment. E, flow cytometry assay probed by DCFDA showing 5 mM NAC stopped ROS generation in MCF-7 exposing to different dose of V9302 (V). F, flow cytometry analysis showing 5 mM NAC led to the upregulation of B7H3 expression in MCF-7 when treated with different concentration of V9302 (V). G, Western blot showing NAC reduced LC3-II expression and led to B7H3 accumulation in MCF-7 when treated with different concentration of V9302 (V). H and I, cytometry analysis showing 5 mM NAC suppressed V9302 (V) induced CD8<sup>+</sup> CTLs activation indicated by the proportion of Granzyme B (GZB)+CD8<sup>+</sup>T cells (H) and CD69+CD8<sup>+</sup>T cells (I). For A, n = 5 independent experiments, for C and H, n = 4 independent experiments, for the rest, n = 3 independent experiments. Data were presented as means ± SD. \*\*p < 0.01; \*\*\*p < 0.001 by Student's t test. NAC, N-acetylcysteine.

## V9302 promotes B7H3 degradation to enhance anti-tumor immunity

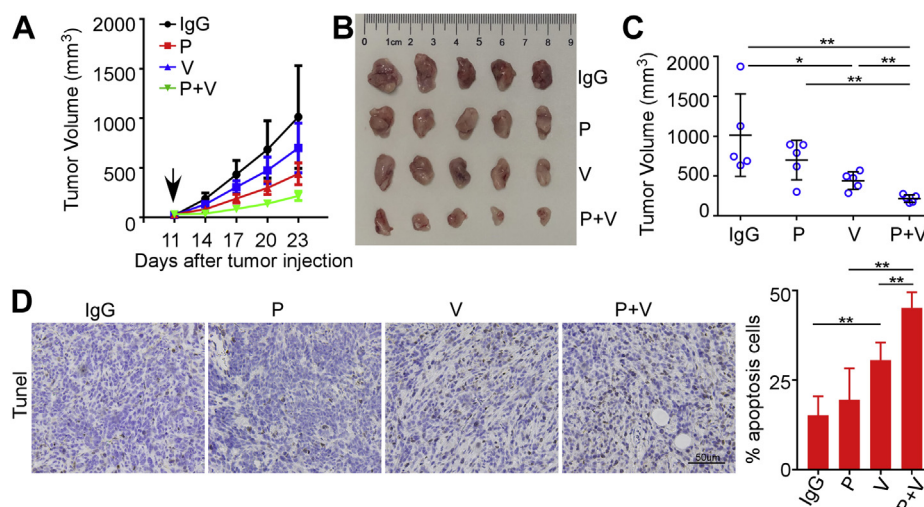


**Figure 5. V9302 improved antitumoral activity of anti-PD-1 immunotherapy in EO771 mouse model.** A, tumor growth curve of EO771-bearing mice with indicated treatments. The black arrow indicates the start of treatment. B, images of EO771 tumors on day 21 with indicated treatments. C, tumor volume of EO771 tumors on day 21. D, tunel staining in EO771 tumor sections treated as indicated. Left, representative images; Right, statistical apoptotic cells percentages in the indicated groups. Scale bars, 50  $\mu$ m. IgG, rat IgG2a; P, anti-PD-1 antibody; V, V9302; P + V, V9302 plus anti-PD-1. For A–C, n = 5 per group, for D, n = 4 per group. Data were presented as means  $\pm$  SD. \* $p$  < 0.05; \*\* $p$  < 0.01 by Student's  $t$  test.

sustained anabolic metabolism demands of proliferating cells. Gln plays pivotal role in macromolecular synthesis (nonessential amino acids, nucleotide, and lipid, etc.) and redox balance by providing both carbon and nitrogen substrates and support of the NADPH production. The roles of Gln metabolism in tumorigenesis have received particular attention recently (39).

Given the critical role of Gln in cancer cell growth and homeostasis, Gln metabolism potentially represents an intervention target for cancer therapy. ASCT2 is the primary and high-affinity transporter of Gln in cancer cells. Preclinical research studies revealed antagonizing or silencing ASCT2 abrogate multiple facets of Gln metabolism and demonstrate dramatic antitumor effects both *in vitro* and *in vivo* (21, 40). Accumulating studies have pointed out that specialized metabolism of cancer cells with the consequence of hypoxia, lactic acid fermentation, and nutrient depletion in tumor tissue not only promotes tumor growth and energetics, but also blocks the generation of an effective antitumor immune response. Therefore, it's not surprising to observe that targeting Gln metabolism remarkably enhances tumor-specific immunity. In our study, we also found blockade of ASCT2 transporter with a small-molecule inhibitor V9302 decreased tumor cell proliferation and increased cell apoptosis. In consideration of the under IC<sub>50</sub> concentration of V9302 used in this study, the antiproliferation effects were indistinct in the animal experiments. Even though, V9302 stimulated a significant antitumor immune response as it increased CD8<sup>+</sup>T-cell activation and quantity in tumor sites and sensitize the potency of anti-PD-1 mAb to block tumor growth.

Glutamine antimetabolites 6-Diazo-5-oxo-L-norleucine (L-DON) or JHU083 (a prodrug form of L-DON) monotherapy leads to a durable tumor remission, which dependent on the enhanced activation and infiltration of CD8<sup>+</sup> T cells and, more generally, Gln antimetabolite alone triggers a powerful immune

memory, as JHU083-treated cancer-removed mice reject the retransplanted new tumors (40). Glutamine antagonists also modulate suppressive myeloid cells in TME. Employment of JHU083 in 4T1-bearing mice markedly inhibited the generation and recruitment of MDSCs and promoted proinflammatory activation and tumor antigen cross-presentation of macrophage to CD8<sup>+</sup> T cells (41). Targeting glutaminase (GLS), which converts Gln into glutamate, is another strategy to block Gln metabolism. Loss of GLS or application of GLS inhibitor CB-839 increased T lymphocytes activation and their infiltration in both a genetically engineered spontaneous mouse TNBC model and orthotopic grafts (42). GLS inhibitor BPTES treatment boosted proinflammatory M1-like activation of macrophages and attenuated protumoral genes expression, therefore eliciting a desirable antitumor immune response (43). V9302 is the first discovered small-molecule antagonist of ASCT2 (26). V9302 blocks glutamine uptake in tumor cells but not in T cells with no obvious impairment of CD8<sup>+</sup> T-cells activation and viability. And in orthotopic EO771 tumors grown in immunocompetent mice, V9302 treatment increased granzyme B-producing CD8<sup>+</sup> CTLs, CD4<sup>+</sup> Th1 T-cell infiltration into tumor core sites and decreased Treg population within tumor environment (42, 44). All these previous studies supported our conclusion that V9302, which affects Gln metabolism in TME not only inhibited tumor growth, but triggered a favorable antitumor immune response.

Though glutamine simultaneously fuels cancer cells and T cells growth, perturbation of glutamine metabolism exposes a previously unexpected difference in cell fate between tumor cells and TILs in TME. A "glutamine steal" scenario has been proposed in which tumor cells outcompeting TILs for the nutrient Gln and impairing their antitumor immune responses (42). Therefore, tumor-preferential targeting of Gln metabolism could reverse this phenomenon and restore TILs functions. It's reported that GLS deletion or application of

V9302 promotes B7H3 degradation to enhance anti-tumor immunity

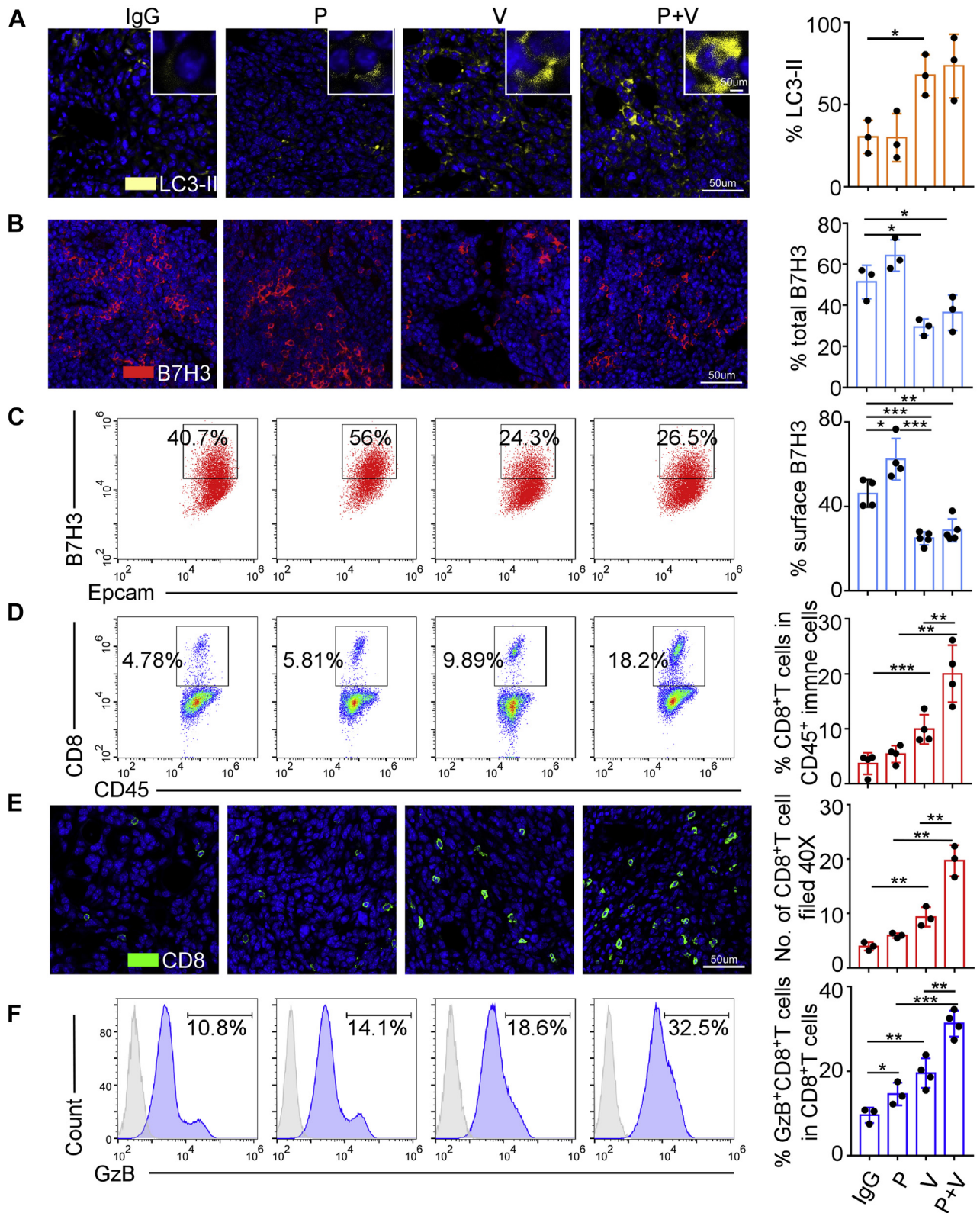


**Figure 6. V9302 enhanced CD8<sup>+</sup> T-cells infiltration and activation by promoting autophagy to reduce B7H3 expression in EO771 mouse model.** A, autophagy marked by LC3-II immunostaining in EO771 tumors treated as indicated. Scale bars, 50  $\mu$ m. B and C, B7H3 expression in EO771 tumors was detected by immunostaining (B) and flow cytometry (C). Scale bars, 50  $\mu$ m. D, flow cytometry analysis of CD8<sup>+</sup> T cells percentage in EO771 tumors treated as indicated. E, representative images of CD8 immunostaining in EO771 tumors treated as indicated. Scale bars, 50  $\mu$ m. F, flow cytometry analysis of GzB<sup>+</sup> CD8<sup>+</sup> T cells percentages in EO771 tumors. IgG, rat IgG2a; P, anti-PD-1 antibody; V, V9302; P + V, V9302 plus anti-PD-1. For A, B, and E n = 3 per group, for C, n = 5 per group, for the rest, n = 4 per group. Data were presented as means  $\pm$  SD. \* $p$  < 0.05; \*\* $p$  < 0.01; \*\*\* $p$  < 0.001 by Student's  $t$  test.

## V9302 promotes B7H3 degradation to enhance anti-tumor immunity

V9302 increased the tumor interstitial Gln concentration, suggesting the improved Gln availability to T cells (26). Furthermore, Gln metabolism inhibitors induce CD8<sup>+</sup>T cells to upregulate alternative transporters, and therefore, immune cells can maintain their Gln utility and not be metabolically disabled of the antitumor immune activities. More importantly, blocking Gln metabolism also relieves the immunosuppressive effects exerted by immune checkpoint molecules. Treatment with L-DON downregulates the expression of TIM-3 and CTLA-4 but not B7H3 in pancreatic cancer and decreases PD-1 expression in the infiltration CD8<sup>+</sup> T cells, resulting in a significantly improved sensitivity to anti-PD-1 immune therapy (45). While application of JHU083 in 4T1 orthotopic transplanted mice decreased IDO expression both in tumor cells and myeloid-derived cells. When mice were treated with JHU083 combined with anti-PD-1 or anti-CTLA4, further tumor regression was achieved than JHU083 monotherapy group (41). In the MC38-bearing mice model, concurrent treatment with Gln antagonist JHU083 and anti-PD-1 promoted proliferation and activation of marker genes' expression in CD8<sup>+</sup> T cells or CTLs and decreased PD-1<sup>+</sup>LAG-3<sup>+</sup> exhausted T cells percentage, leading to remarkably improved antitumor effects compared with anti-PD-1 monotherapy (40). Taken together, Gln antimetabolites, transport antagonists, and GLS inhibitors are all reported to synergize with immune checkpoint blockade by various mechanisms. In our present study, we also proved that Gln transporter blocker V9302 could sensitize anti-PD-1 efficacy even in the "immune cold" luminal-type breast cancer and anti-PD-1/PD-L1-resistant 4T1 (46) syngeneic murine cancer models with increased CD8<sup>+</sup> T-cell infiltration and activation.

Unlike lung cancer, skin cancer, and bladder cancer, most breast cancers are not inherently immunogenic, among which TNBC is considered the most immunogenic subtype with higher PD-1/PD-L1 expression, more TILs infiltration, and higher TMB. Though patients with PD-L1<sup>+</sup> mTNBC have experienced benefit from the combination of anti-PD-1/PD-L1 antibody with chemotherapy agents (7), this population represents only a small proportion of patients with breast cancer. Therefore, biomarkers to predict immunotherapy efficacy and alternative combinational treatment strategy should be explored. B7H3 is specifically overexpressed in breast cancer compared with normal breast tissue and benign lesions (47). It has been considered as a T-cell coinhibitory molecule recently and tends to be associated with low density of TILs in TME (48). In several preclinical studies, including breast cancer, ovarian cancer, non-small cell lung cancer (NSCLC), and head and neck squamous-cell carcinoma, anti-B7H3 therapy reduced the tumor burden related to the enhanced activation of CTLs (49–51). Therefore, B7H3 may be an attractive target for cancer immunotherapy. In this study, when further investigating the underlying mechanism of V9302-upregulated immunotherapy response, we found for the first time that V9302 employment decreased the expression of B7H3, which might mediate inhibitory signals to blunt T-cell activity in breast cancers refractory to PD-1 blockade therapy. These results were consistent with the observation in NSCLC that

anti-B7H3 blockade alone increased CD8<sup>+</sup> TILs and restored their cytotoxicity. When combined with anti-PD-L1 antibody, anti-B7H3 further enhanced the antitumor reaction (17, 52). In ovarian cancer, which has a lower PD-L1 level and is insensitive to anti-PD-1/PD-L1 blockade therapy, B7H3 played a dominant role in modulating the immunosuppressive TME. Irrespective of the expression of PD-L1, the decrease of B7H3 in tumor cells enhanced T-cell effector functions (53). All these results highlighted B7H3 combined with anti-PD-1/PD-L1 as a potential therapeutic strategy to reinvigorate T cell functions and unleash antitumor immunity in breast cancer patients resistant to the PD-L1/PD-1 monotherapy.

Another novel conclusion of this study is that we found that V9302 decreased B7H3 expression by promoting its autophagy-lysosome pathway-mediated degradation. Mortimore and Schworer in 1977 observed that amino acid deprivation induces the accumulation of autophagosomes in perfused rat liver, providing the first evidence that amino acids regulate autophagy. Enhanced autophagy following V9302 exposure was noticed in multiple cell lines, which was not unexpected when considering the relationship between Gln withdrawal, imbalanced ROS and NADPH production, and autophagy (54).

V9302 didn't affect the transcriptional activity of B7H3 mRNA; therefore, we investigated if Gln metabolism regulated its degradation by using several inhibitors targeting intracellular protein-degradation pathways. The proteasome inhibitor MG132 elevated B7H3 expression in the absence of V9302, while after the application of different concentrations of V9302, MG132 couldn't stop the decrease of B7H3. In contrast, autophagy inhibitor Baf A1 significantly inhibited V9302-induced B7H3 degradation. Furthermore, block of ROS-autophagy pathway by NAC rescued the expression of B7H3 protein in the presence of V9302. All this illustrated V9302 initiates the autophagy–lysosome pathway to regulate B7H3 expression and the following immune regulatory functions.

Recent studies have shown that the accumulated ROS could not only initiate autophagosome formation and autophagic degradation of damaged/oxidized proteins, but also induce the disposal of dysfunctional mitochondria, the major ROS-producing organelle, by autophagy called mitophagy to decrease the levels of ROS. The onset of mitophagy requires two steps: induction of general autophagy, which utilizes the same core autophagy machinery, and selective autophagic cargo recognition of damaged mitochondria mediated by PINK1-PRKN pathway, or mitochondrial proteins BNIP3, BNIP3L/NIX, and FUNDC1. These studies suggested that active removal of existing oxidized proteins or damaged organelles shares the same autophagy machinery, but with the specific cargo recognition system. They can take place in response to stress simultaneously. Whether V9302 elicits mitophagy, and what are the effects of mitophagy exerted on redox balance and autophagy-mediated B7H3 degradation need to be further investigated (55–57). In summary, we reported a novel mechanism of glutamine metabolism regulated antitumor immune response in breast cancer. These results not only displayed that blockade of Gln transporter decreased the expression of T-cell coinhibitory molecule B7H3 by ROS-

## V9302 promotes B7H3 degradation to enhance anti-tumor immunity

mediated autophagy degradation pathway, but also illustrated the promising combination immunotherapy strategy of anti-PD-1 with anti-B7H3 to replenish CD8<sup>+</sup> T-cell infiltration and augment antitumor immune response (Fig. 7). So far, B7H3 mAb enoblituzumab plus anti-PD-1 mAb has been evaluated in phase I clinical trial in patients with bladder cancer, melanoma, squamous cell carcinoma of the head and neck, and lung cancer and showed antitumor effects and increased TILs infiltration (58). This has generated great interest in combining anti-PD-1/PD-L1 mAb with B7H3 blockades (anti-B7H3 mAb or V9302) immunotherapy strategies for "immune-desert" or "innate immune-inactivated" breast cancer clusters to transform "cold tumors" into "hot tumors" and benefit patients with metastatic or advanced

breast cancer. There is still a lot of basic research and clinical trials needed to confirm and optimize the benefits of this combination immunotherapy in breast cancer.

### Experimental procedures

#### Patients and tissue samples

Tumor samples were obtained from 65 patients with invasive breast carcinoma at the Sixth Affiliated Hospital, Sun Yat-sen University (Guangzhou, China) between 2020 and 2021, and were used for LC3-II, B7H3, and CD8 immunohistochemistry staining and correlation analysis. Peripheral blood samples were obtained in 2021 and used for primary CD8<sup>+</sup> T-cells isolation and analysis. All tumor samples were

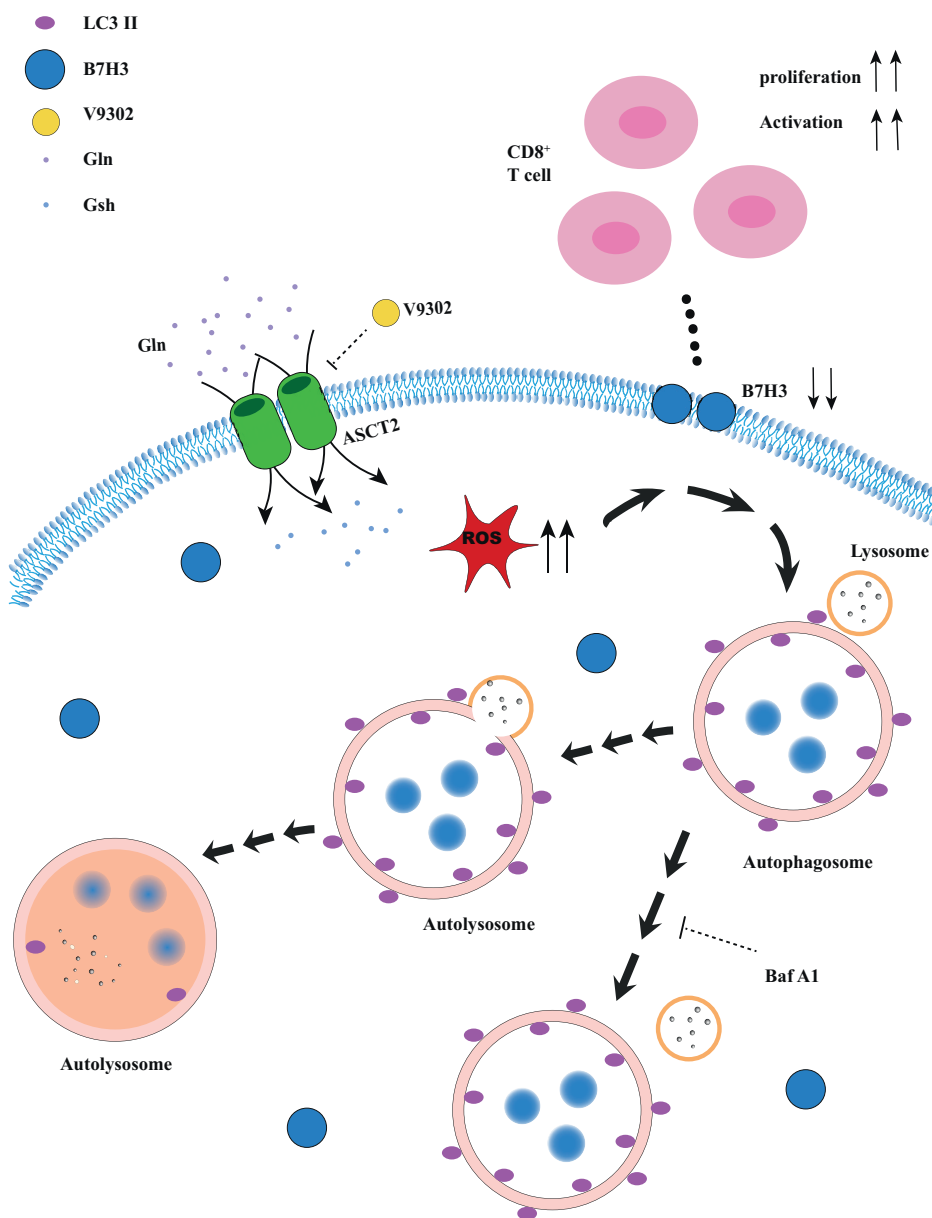


Figure 7. An overview schematic demonstrating that V9302 enhanced CD8<sup>+</sup>T cell activation by promoting B7H3 degradation via autophagy-lysosome pathway and potentiated the antitumor effect of anti-PD-1 immune therapy.

## V9302 promotes B7H3 degradation to enhance anti-tumor immunity

collected from patients who had provided informed consent, and all related procedures were performed with the approval of the internal review and ethics board of the Sixth Affiliated Hospital, Sun Yat-sen University.

### Immunohistochemistry (IHC) and immunofluorescence (IF)

Paraffin-embedded samples were cut into 5  $\mu\text{m}$  sections and deparaffinized. Specimens were incubated at 4  $^{\circ}\text{C}$  overnight with antibodies against human LC3-II (Cell Signaling Technology, 83506), B7H3 (Cell Signaling Technology, 14058), CD8 (ZSGB-BIO, ZA-0508), and Ki67 (Abcam, ab15580) or against mouse LC3-II (Abcam, ab48394), B7H3 (Abcam, ab134161), and CD8 $\alpha$  (Cell Signaling Technology, CST, 98941). Specimens were then washed by PBS and stained with anti-mouse/rabbit IHC secondary antibody kit or incubated with Alexa Fluor secondary antibodies. TUNEL assay (KeyGene Biotech, KGA7061 and Beyotime, C1098) for the detection of cell apoptosis was stained following the instructions of the manufacturer. The staining score of B7H3 was determined as the product of the proportion of positive stained cells and intensity as previously described (59), and 5 to 10 areas per tumor sample were randomly selected for analysis. The LC3-II antibody was used to detect the autophagosomes, which could be seen as LC3-II dots. Autophagosomes of tissue sections were calculated by the average number of autophagic dots in each cell to represent its autophagic level. CD8 $^{+}$  T-cells infiltration was evaluated as the percentage of CD8 positively stained lymphocytes to tumor center following pathologist designation of the tumor area (60).

### Cell lines and reagents

MCF-7, T47D, BT-474, MDA-MB-231, and BT-549 breast cancer cell lines were obtained from the American Type Culture Collection (ATCC) and cultured according to the recommended protocols. Cells were treated with lysosomal inhibition bafilomycin A1 (MedChemExpress, HY-100558) for 6 h to test B7H3 and LC3-II expression. Increasing concentration of V9302 (MedChemExpress, HY-112683) was applied to tumor cells for 24 h, unless otherwise marked in the figure labels, in the presence or absence of N-acetyl-cysteine (NAC) (MedChemExpress, HY-B0215) for cytotoxicity assay, apoptosis analysis, ROS detection, Western blot, and tumor lysis collection, or with or without MG132 (Sigma, M8699) to test B7H3 expression.

### Cell viability assay and apoptosis assay

MCF-7 and BT-474 were seeded in 96-well plates ( $1 \times 10^4$  per well) or 24-well plates ( $5 \times 10^4$  per well) and treated with 0, 0.5, 1, 2  $\mu\text{g}/\text{ml}$  V9302 for 24 h. Then, cell viability was detected using trypan blue exclusion assay according to the manufacturer's recommendation, and cell apoptosis was detected by Annexin V/PI apoptosis kit (Multisciences, 70-AP101-100) and analyzed by flow cytometry (Beckman CytoFLEX Flow cytometer).

### Measurement of ROS

Intracellular ROS level was measured using CM-H2DCFDA (Thermo Fisher, C6827) as a probe and assessed by flow cytometry in accordance with the manufacturer's protocol.

### Western blot analysis

For protein extraction, cells were homogenized by IP lysis buffer (Thermo Fisher, 87787) with a proteinase inhibitor cocktail (Thermo Fisher, 78442). Total protein was quantified using the Pierce BCA Protein Assay Kit (Thermo Fisher, 23227). Equal amounts of the lysates were separated by 10% SDS-PAGE and electro-transferred to nitrocellulose membranes. After being blocked with TBS/0.05% Tween-20/5% skim milk, the membranes were probed with antibodies against LC3-II (Cell Signaling Technology, 83506), B7H3 (Cell Signaling Technology, 14058), PARP (Cell Signaling Technology, 9532), cleaved PARP (Cell Signaling Technology, 5625), Caspase3 (Cell Signaling Technology, 9662), cleaved Caspase3 (Cell Signaling Technology, 9664), or GAPDH (Proteintech, HRP-60004). Peroxidase-conjugated anti-rabbit antibody and anti-mouse antibody were used as secondary antibodies, and signals were captured by chemiluminescence (Syngene).

### Isolation of primary tumor cells from tumor-bearing mice

Briefly, tumor tissues were exhaustively flushed with PBS, minced into small (1–2 mm in diameter) pieces, and digested with 2% FBS DMEM containing 2 mg/ml collagenase IV (Sigma, C5138) at 37  $^{\circ}\text{C}$  for 30 min. Cells were sequentially filtered through a 500  $\mu\text{m}$  mesh and then 100 and 40  $\mu\text{m}$  cell strainers. Cell suspension were further washed twice and stained with CD45 (Biolegend, 103114) and CD8 (Biolegend, 100737), CD8 and GZB (Biolegend, 515403), or EPCAM (Biolegend, 118206) and B7H3 (Biolegend, 135613) antibodies for flow cytometry analysis. The gating strategies were shown in Figs. S7 and S8.

### Generation of matured DCs and CD8 $^{+}$ CTLs from peripheral blood mononuclear cells

Peripheral blood mononuclear cells from healthy donors were collected by Percoll density gradient centrifugation as previously described (61). DCs were generated by culturing monocytes in DMEM with 10% FBS, 50 ng/ml GM-CSF (PeproTech, 300-03), 20 ng/ml IL-4 (PeproTech, 200-04) for 5 days. Afterward, DCs ( $1 \times 10^6$  cells/well in a 24-well plate) were incubated with 100 ng/ml LPS (Sigma, L2630) and 500 U/ml IFN- $\gamma$  (PeproTech, 300-02) for 48 h to generate mature DCs. Allogeneic tumor cell lysates have been used as a source of antigens for pulsing DCs (62). Briefly,  $3 \times 10^6$  tumor cells (MCF-7 or BT-474) with different treatments as indicated in "Cell lines and reagents" section were resuspended in 1 ml serum-free DMEM and lysed by five freeze/thaw cycles. The obtained lysates were centrifuged at 12,000g for 15 min at 4  $^{\circ}\text{C}$  to remove cell debris, and the supernatants were loaded to DCs (200  $\mu\text{g}$  protein/ $1 \times 10^6$  cells/ml) for 24 h.

CD8 $^{+}$  T cells were sorted by CD8 $^{+}$  T Cell Isolation Kit (Miltenyi Biotec, 130-096-495) and maintained in RPMI 1640 medium with 10% FBS, 25 U/ml IL-2 (PeproTech, 200-02-10UG). Then cells ( $5 \times 10^6$  cells/well) were cocultured with tumor lysates pulsed DCs (5:1) in 24-well plate for 5 days to obtain CTLs. Fluorescence-labeled antibodies against CD8

(Biolegend, 344705), granzyme B (Biolegend, 515403), and CD69 (Biolegend, 310909) were evaluated by flow cytometry and analyzed using FlowJo software.

### Animal studies

All animal studies were reviewed and approved by the Institutional Animal Care and Use Committee of Sun Yat-sen University. For syngeneic murine models,  $5 \times 10^6$  EO771 and  $2 \times 10^5$  4T1 breast cancer cells were inoculated into the fat pad of female 4 to 6-week-old C57 and BALB/c mice, respectively. When tumors reached a volume of 20 mm<sup>3</sup>, mice were randomized to receive one of the following treatments by peritoneal injection (*i.p.*) (for 2 weeks): rat IgG2a (bioxcell, 40 mg/kg, twice a week), anti-PD-1 antibody (bioxcell, 10 mg/kg, twice a week), V9302 (MCE, 75 mg/kg, everyday), or V9302 plus anti-PD-1. Tumor growth was monitored every 3 days by measuring tumor length (L) and width (W). Tumor volume (V) was then calculated using the formula,  $V = 1/2 \times L \times W^2$ . When the allografts reached 1.5 cm in diameter, the grafts were dissected for further IHC, IF, and flow cytometry evaluation.

### Statistical analysis

A completely randomized, balanced design was used for all experiments. Chi-square analysis was used to analyze the relationship between B7H3 expression, LC3-II dots, CD8<sup>+</sup>T-cell infiltration, and clinicopathological status. Data for Figure 1, D and E with discrete variables were compared by means of the Mann–Whitney U test. Other comparison groups have the similar variance. One-way ANOVA was used to compare the effects of different concentrations of V9302. Two-tailed student's *t* test was used to test the significance between two groups. All statistical analysis was done using Graphpad Prism 7.0. *p* value less than 0.05 was considered significant. Standard deviation (SD) for a minimum of three independent experiments was used to measure the variation as indicated in the figure legends.

### Ethics statement

This study was approved and supervised by the internal review and ethics board of the Sixth Affiliated Hospital, Sun Yat-sen University. All samples were collected with signed informed consent. The treatment of animals in all experiments conforms to the Institutional Animal Care and Use Committee of Sun Yat-sen University.

### Data availability

The Curtis dataset was obtained from public Oncomine portal ([www.oncomine.org](http://www.oncomine.org)). All other remaining data are included in the article and supplementary files.

**Acknowledgments**—We thank Dr Jianjian Wu for assistance with sample staining. We thank all the patients who agreed to participate in the trial. This work was supported by grants from Guangdong Science and Technology Department (2020A1515010425, 2019A1515010146), Guangzhou Science and Technology Project

(805275295029), and National Natural Science Foundation of China (81672622), Dongguan Science and Technology of Social Development Program (20211800904582).

**Author contributions**—Q. L., D. Z., Y. L., and H. L. conceptualization; J. Y. data curation; Q. L., X. Z., and W. Y. formal analysis; Y. L. and H. L. funding acquisition; Q. L., X. Z., F. Q., X. F., and X. H. investigation; W. Y. and Z. L. methodology; C. W. resources; D. Z. supervision; X. Z., W. Y., and S. L. validation; X. Z. visualization; Q. L. and Y. L. writing—original draft; H. L. writing—review and editing.

**Conflict of interest**—The authors declare there is no conflict of interest with the contents of this article.

**Abbreviations**—The abbreviations used are: B7H3, B7 homolog 3; Baf A1, bafilomycin A1; ER<sup>+</sup>, estrogen receptor positive; Gln, glutamine; GLS, glutaminase; GzB, granzyme B; IFN, interferon; IHC, immunohistochemistry; L-DON, 6-Diazo-5-oxo-L-norleucine; mAb, monoclonal antibody; NAC, N-acetylcysteine; NSCLC, non-small cell lung cancer; ORR, objective response rate; ROS, reactive oxygen species; Tem, T effector memory; TIL, tumor-infiltration lymphocyte; TMB, tumor mutation burden; TME, tumor micro-environment; TNBC, triple-negative breast cancer; Treg, regulatory T cell.

### References

- Sung, H., Ferlay, J., Siegel, R. L., Laversanne, M., Soerjomataram, I., Jemal, A., and Bray, F. (2021) Global Cancer Statistics 2020: GLOBOCAN estimates of incidence and mortality worldwide for 36 cancers in 185 countries. *CA Cancer J. Clin.* **71**, 209–249
- Sanmamed, M. F., and Chen, L. (2018) A paradigm shift in cancer immunotherapy: From enhancement to normalization. *Cell* **175**, 313–326
- Dirix, L. Y., Takacs, I., Jerusalem, G., Nikolinakos, P., Arkenau, H. T., Forero-Torres, A., Boccia, R., Lippman, M. E., Somer, R., Smakal, M., Emens, L. A., Hrinchenko, B., Edenfield, W., Gurtler, J., von Heydebreck, A., *et al.* (2018) Avelumab, an anti-PD-L1 antibody, in patients with locally advanced or metastatic breast cancer: A phase 1b JAVELIN solid tumor study. *Breast Cancer Res. Treat.* **167**, 671–686
- Emens, L. A., Cruz, C., Eder, J. P., Braiteh, F., Chung, C., Tolaney, S. M., Kuter, I., Nanda, R., Cassier, P. A., Delord, J. P., Gordon, M. S., ElGaby, E., Chang, C. W., Sarkar, I., Grossman, W., *et al.* (2019) Long-term clinical outcomes and biomarker analyses of atezolizumab therapy for patients with metastatic triple-negative breast cancer: A phase 1 study. *JAMA Oncol.* **5**, 74–82
- Nanda, R., Chow, L. Q., Dees, E. C., Berger, R., Gupta, S., Geva, R., Puszta, L., Pathiraja, K., Aktan, G., Cheng, J. D., Karantza, V., and Buisseret, L. (2016) Pembrolizumab in patients with advanced triple-negative breast cancer: Phase 1b KEYNOTE-012 study. *J. Clin. Oncol.* **34**, 2460–2467
- Rugo, H. S., Delord, J. P., Im, S. A., Ott, P. A., Piha-Paul, S. A., Bedard, P. L., Sachdev, J., Le Tourneau, C., van Brummelen, E. M. J., Varga, A., Salgado, R., Loi, S., Saraf, S., Pietrangolo, D., Karantza, V., *et al.* (2018) Safety and antitumor activity of pembrolizumab in patients with estrogen receptor-positive/human epidermal growth factor receptor 2-negative advanced breast cancer. *Clin. Cancer Res.* **24**, 2804–2811
- Schmid, P., Rugo, H. S., Adams, S., Schneeweiss, A., Barrios, C. H., Iwata, H., Dieras, V., Henschel, V., Molinero, L., Chui, S. Y., Maiya, V., Husain, A., Winer, E. P., Loi, S., Emens, L. A., *et al.* (2020) Atezolizumab plus nab-paclitaxel as first-line treatment for unresectable, locally advanced or metastatic triple-negative breast cancer (IMpassion130): Updated efficacy results from a randomised, double-blind, placebo-controlled, phase 3 trial. *Lancet Oncol.* **21**, 44–59
- Schmid, P., Cortes, J., Puszta, L., McArthur, H., Kummel, S., Bergh, J., Denkert, C., Park, Y. H., Hui, R., Harbeck, N., Takahashi, M., Foukakis, T.,

## V9302 promotes B7H3 degradation to enhance anti-tumor immunity

- Fasching, P. A., Cardoso, F., Untch, M., *et al.* (2020) Pembrolizumab for early triple-negative breast cancer. *N. Engl. J. Med.* **382**, 810–821
- Munoz-Rojas, A. R., and Mathis, D. (2021) Tissue regulatory T cells: Regulatory chameleons. *Nat. Rev. Immunol.* **21**, 597–611
  - Hegde, S., Leader, A. M., and Merad, M. (2021) MDSC: Markers, development, states, and unaddressed complexity. *Immunity* **54**, 875–884
  - Sharma, P., Hu-Lieskovan, S., Wargo, J. A., and Ribas, A. (2017) Primary, adaptive, and acquired resistance to cancer immunotherapy. *Cell* **168**, 707–723
  - Chen, G., Tu, Y., Aladelusi, T. O., Zhao, S., Chen, J., Jin, L., and Zhu, D. (2020) Knocking down B7H3 expression enhances cell proliferation of SHEDs via the SHP1/AKT signal axis. *Biochem. Biophys. Res. Commun.* **531**, 282–289
  - Ganesan, B., Parameswaran, S., Sharma, A., and Krishnakumar, S. J. S. (2020) Clinical relevance of B7H3 expression in retinoblastoma. *Sci. Rep.* **10**, 10185
  - Zhu, X. W., Wang, J., Zhu, M. X., Wang, Y. F., Yang, S. Y., and Ke, X. Y. (2019) MicroRNA-506 inhibits the proliferation and invasion of mantle cell lymphoma cells by targeting B7H3. *Biochem. Biophys. Res. Commun.* **508**, 1067–1073
  - Seaman, S., Zhu, Z., Saha, S., Zhang, X. M., Yang, M. Y., Hilton, M. B., Morris, K., Szot, C., Morris, H., Swing, D. A., Tessarollo, L., Smith, S. W., Degrado, S., Borokin, D., Jain, N., *et al.* (2017) Eradication of tumors through simultaneous ablation of CD276/B7-H3-positive tumor cells and tumor vasculature. *Cancer Cell* **31**, 501–515.e8
  - Yang, S., Wei, W., and Zhao, Q. (2020) B7-H3, a checkpoint molecule, as a target for cancer immunotherapy. *Int. J. Biol. Sci.* **16**, 1767–1773
  - Yonesaka, K., Haratani, K., Takamura, S., Sakai, H., Kato, R., Takegawa, N., Takahama, T., Tanaka, K., Hayashi, H., Takeda, M., Kato, S., Mae-nishi, O., Sakai, K., Chiba, Y., Okabe, T., *et al.* (2018) B7-H3 negatively modulates CTL-mediated cancer immunity. *Clin. Cancer Res.* **24**, 2653–2664
  - Zhang, H., Cui, K., Yao, S., Yin, Y., Liu, D., and Huang, Z. (2021) Comprehensive molecular and clinical characterization of SLC1A5 in human cancers. *Pathol. Res. Pract.* **224**, 153525
  - Bernhardt, S., Bayerlova, M., Vetter, M., Wachter, A., Mitra, D., Hanf, V., Lantzsch, T., Uleer, C., Peschel, S., John, J., Buchmann, J., Weigert, E., Burrig, K. F., Thomssen, C., Korf, U., *et al.* (2017) Proteomic profiling of breast cancer metabolism identifies SHMT2 and ASCT2 as prognostic factors. *Breast Cancer Res.* **19**, 112
  - El-Ansari, R., Craze, M. L., Alfarsi, L., Soria, D., Diez-Rodriguez, M., Nolan, C. C., Ellis, I. O., Rakha, E. A., and Green, A. R. (2019) The combined expression of solute carriers is associated with a poor prognosis in highly proliferative ER+ breast cancer. *Breast Cancer Res. Treat.* **175**, 27–38
  - Wang, Q., Hardie, R. A., Hoy, A. J., van Geldermalsen, M., Gao, D., Fazli, L., Sadowski, M. C., Balaban, S., Schreuder, M., Nagarajah, R., Wong, J. J., Metierre, C., Pinello, N., Otte, N. J., Lehman, M. L., *et al.* (2015) Targeting ASCT2-mediated glutamine uptake blocks prostate cancer growth and tumour development. *J. Pathol.* **236**, 278–289
  - Ren, W., Liu, G., Yin, J., Tan, B., Wu, G., Bazer, F. W., Peng, Y., and Yin, Y. (2017) Amino-acid transporters in T-cell activation and differentiation. *Cell Death Dis.* **8**, e2655
  - Nakaya, M., Xiao, Y., Zhou, X., Chang, J. H., Chang, M., Cheng, X., Blonska, M., Lin, X., and Sun, S. C. (2014) Inflammatory T cell responses rely on amino acid transporter ASCT2 facilitation of glutamine uptake and mTORC1 kinase activation. *Immunity* **40**, 692–705
  - Ma, G., Liang, Y., Chen, Y., Wang, L., Li, D., Liang, Z., Wang, X., Tian, D., Yang, X., and Niu, H. (2020) Glutamine deprivation induces PD-L1 expression via activation of EGFR/ERK/c-Jun signaling in renal cancer. *Mol. Cancer Res.* **18**, 324–339
  - Byun, J. K., Park, M., Lee, S., Yun, J. W., Lee, J., Kim, J. S., Cho, S. J., Jeon, H. J., Lee, I. K., Choi, Y. K., and Park, K. G. (2020) Inhibition of glutamine utilization synergizes with immune checkpoint inhibitor to promote antitumor immunity. *Mol. Cell* **80**, 592–606.e8
  - Schulte, M., Fu, A., Zhao, P., Li, J., Geng, L., Smith, S., Kondo, J., Coffey, R., Johnson, M., Rathmell, J., Sharick, J., Skala, M., Smith, J., Berlin, J., Washington, M., *et al.* (2018) Pharmacological blockade of ASCT2-dependent glutamine transport leads to antitumor efficacy in preclinical models. *Nat. Med.* **24**, 194–202
  - Levy, J. M. M., Towers, C. G., and Thorburn, A. (2017) Targeting autophagy in cancer. *Nat. Rev. Cancer* **17**, 528–542
  - Signorelli, S., Tarkowski, L. P., Van den Ende, W., and Bassham, D. C. (2019) Linking autophagy to abiotic and biotic stress responses. *Trends Plant Sci.* **24**, 413–430
  - Mehazri, L., Shpungin, S., Bel, S., and Nir, U. (2021) Loss of fer jeopardizes metabolic plasticity and mitochondrial homeostasis in lung and breast carcinoma cells. *Int. J. Mol. Sci.* **22**, 3387
  - Ewens, A., Mihich, E., and Ehrke, M. J. (2005) Distant metastasis from subcutaneously grown E0771 medullary breast adenocarcinoma. *Anti-cancer Res.* **25**, 3905–3915
  - Clarke, R., Jones, B. C., Sevigny, C. M., Hilakivi-Clarke, L. A., and Sengupta, S. (2021) Experimental models of endocrine responsive breast cancer: Strengths, limitations, and use. *Cancer Drug Resist.* **4**, 762–783
  - Le Naour, A., Rossary, A., and Vasson, M. P. (2020) EO771, is it a well-characterized cell line for mouse mammary cancer model? Limit and uncertainty. *Cancer Med.* **9**, 8074–8085
  - Zhou, F., Wang, M., Luo, T., Qu, J., and Chen, W. R. (2021) Photo-activated chemo-immunotherapy for metastatic cancer using a synergistic graphene nanosystem. *Biomaterials* **265**, 120421
  - Loi, S., Sirtaine, N., Piette, F., Salgado, R., Viale, G., Van Eenoo, F., Rouas, G., Francis, P., Crown, J. P., Hitre, E., de Azambuja, E., Quinaux, E., Di Leo, A., Michiels, S., Piccart, M. J., *et al.* (2013) Prognostic and predictive value of tumor-infiltrating lymphocytes in a phase III randomized adjuvant breast cancer trial in node-positive breast cancer comparing the addition of docetaxel to doxorubicin with doxorubicin-based chemotherapy: Big 02-98. *J. Clin. Oncol.* **31**, 860–867
  - Adams, S., Gray, R. J., Demaria, S., Goldstein, L., Perez, E. A., Shulman, L. N., Martino, S., Wang, M., Jones, V. E., Saphner, T. J., Wolff, A. C., Wood, W. C., Davidson, N. E., Sledge, G. W., Sparano, J. A., *et al.* (2014) Prognostic value of tumor-infiltrating lymphocytes in triple-negative breast cancers from two phase III randomized adjuvant breast cancer trials: ECOG 2197 and ECOG 1199. *J. Clin. Oncol.* **32**, 2959–2966
  - Loi, S., Michiels, S., Salgado, R., Sirtaine, N., Jose, V., Fumagalli, D., Kellokumpu-Lehtinen, P. L., Bono, P., Kataja, V., Desmedt, C., Piccart, M. J., Loibl, S., Denkert, C., Smyth, M. J., Joensuu, H., *et al.* (2014) Tumor infiltrating lymphocytes are prognostic in triple negative breast cancer and predictive for trastuzumab benefit in early breast cancer: Results from the FinHER trial. *Ann. Oncol.* **25**, 1544–1550
  - Denkert, C., von Minckwitz, G., Brase, J. C., Sinn, B. V., Gade, S., Kronenwett, R., Pfitzner, B. M., Salat, C., Loi, S., Schmitt, W. D., Schem, C., Fisch, K., Darb-Esfahani, S., Mehta, K., Sotiriou, C., *et al.* (2015) Tumor-infiltrating lymphocytes and response to neoadjuvant chemotherapy with or without carboplatin in human epidermal growth factor receptor 2-positive and triple-negative primary breast cancers. *J. Clin. Oncol.* **33**, 983–991
  - Bhutia, Y. D., Babu, E., Ramachandran, S., and Ganapathy, V. (2015) Amino acid transporters in cancer and their relevance to “glutamine addiction”: Novel targets for the design of a new class of anticancer drugs. *Cancer Res.* **75**, 1782–1788
  - Yang, W. H., Qiu, Y., Stamatatos, O., Janowitz, T., and Lukey, M. J. (2021) Enhancing the efficacy of glutamine metabolism inhibitors in cancer therapy. *Trends Cancer* **7**, 790–804
  - Leone, R. D., Zhao, L., Englert, J. M., Sun, I. M., Oh, M. H., Sun, I. H., Arwood, M. L., Bettencourt, I. A., Patel, C. H., Wen, J., Tam, A., Blosser, R. L., Prchalova, E., Alt, J., Rais, R., *et al.* (2019) Glutamine blockade induces divergent metabolic programs to overcome tumor immune evasion. *Science* **366**, 1013–1021
  - Oh, M. H., Sun, I. H., Zhao, L., Leone, R. D., Sun, I. M., Xu, W., Collins, S. L., Tam, A. J., Blosser, R. L., Patel, C. H., Englert, J. M., Arwood, M. L., Wen, J., Chan-Li, Y., Tenora, L., *et al.* (2020) Targeting glutamine metabolism enhances tumor-specific immunity by modulating suppressive myeloid cells. *J. Clin. Invest.* **130**, 3865–3884
  - Edwards, D. N., Ngwa, V. M., Raybuck, A. L., Wang, S., Hwang, Y., Kim, L. C., Cho, S. H., Paik, Y., Wang, Q., Zhang, S., Manning, H. C., Rathmell, J. C., Cook, R. S., Boothby, M. R., and Chen, J. (2021) Selective glutamine

- metabolism inhibition in tumor cells improves antitumor T lymphocyte activity in triple-negative breast cancer. *J. Clin. Invest.* **131**, e140100
43. Liu, P. S., Wang, H., Li, X., Chao, T., Teav, T., Christen, S., Di Conza, G., Cheng, W. C., Chou, C. H., Vavakova, M., Muret, C., Debackere, K., Mazzone, M., Huang, H. D., Fendt, S. M., *et al.* (2017) Alpha-ketoglutarate orchestrates macrophage activation through metabolic and epigenetic reprogramming. *Nat. Immunol.* **18**, 985–994
  44. Johnson, M. O., Wolf, M. M., Madden, M. Z., Andrejeva, G., Sugiura, A., Contreras, D. C., Maseda, D., Liberti, M. V., Paz, K., Kishton, R. J., Johnson, M. E., de Cubas, A. A., Wu, P., Li, G., Zhang, Y., *et al.* (2018) Distinct regulation of Th17 and Th1 cell differentiation by glutaminase-dependent metabolism. *Cell* **175**, 1780–1795.e19
  45. Sharma, N. S., Gupta, V. K., Garrido, V. T., Hadad, R., Durden, B. C., Kesh, K., Giri, B., Ferrantella, A., Dudeja, V., Saluja, A., and Banerjee, S. (2020) Targeting tumor-intrinsic hexosamine biosynthesis sensitizes pancreatic cancer to anti-PD1 therapy. *J. Clin. Invest.* **130**, 451–465
  46. Kim, K., Skora, A. D., Li, Z., Liu, Q., Tam, A. J., Blosser, R. L., Diaz, L. A., Jr., Papadopoulos, N., Kinzler, K. W., Vogelstein, B., and Zhou, S. (2014) Eradication of metastatic mouse cancers resistant to immune checkpoint blockade by suppression of myeloid-derived cells. *Proc. Natl. Acad. Sci. U. S. A.* **111**, 11774–11779
  47. Bachawal, S. V., Jensen, K. C., Wilson, K. E., Tian, L., Lutz, A. M., and Willmann, J. K. (2015) Breast cancer detection by B7-H3-targeted ultrasound molecular imaging. *Cancer Res.* **75**, 2501–2509
  48. Andrews, L. P., Yano, H., and Vignali, D. A. A. (2019) Inhibitory receptors and ligands beyond PD-1, PD-L1 and CTLA-4: Breakthroughs or backups. *Nat. Immunol.* **20**, 1425–1434
  49. Qin, S., Xu, L., Yi, M., Yu, S., Wu, K., and Luo, S. (2019) Novel immune checkpoint targets: Moving beyond PD-1 and CTLA-4. *Mol. Cancer* **18**, 155
  50. Lee, Y. H., Martin-Orozco, N., Zheng, P., Li, J., Zhang, P., Tan, H., Park, H. J., Jeong, M., Chang, S. H., Kim, B. S., Xiong, W., Zang, W., Guo, L., Liu, Y., Dong, Z. J., *et al.* (2017) Inhibition of the B7-H3 immune checkpoint limits tumor growth by enhancing cytotoxic lymphocyte function. *Cell Res.* **27**, 1034–1045
  51. Wang, C., Li, Y., Jia, L., Kim, J. K., Li, J., Deng, P., Zhang, W., Krebsbach, P. H., and Wang, C. Y. (2021) CD276 expression enables squamous cell carcinoma stem cells to evade immune surveillance. *Cell Stem Cell* **28**, 1597–1613.e7
  52. Liu, J., Yang, S., Cao, B., Zhou, G., Zhang, F., Wang, Y., Wang, R., Zhu, L., Meng, Y., Hu, C., Liang, H., Lin, X., Zhu, K., Chen, G., Luo, K. Q., *et al.* (2021) Targeting B7-H3 via chimeric antigen receptor T cells and bispecific killer cell engagers augments antitumor response of cytotoxic lymphocytes. *J. Hematol. Oncol.* **14**, 21
  53. Cai, D., Li, J., Liu, D., Hong, S., Qiao, Q., Sun, Q., Li, P., Lyu, N., Sun, T., Xie, S., Guo, L., Ni, L., Jin, L., and Dong, C. (2020) Tumor-expressed B7-H3 mediates the inhibition of antitumor T-cell functions in ovarian cancer insensitive to PD-1 blockade therapy. *Cell. Mol. Immunol.* **17**, 227–236
  54. Tan, H. W. S., Sim, A. Y. L., and Long, Y. C. (2017) Glutamine metabolism regulates autophagy-dependent mTORC1 reactivation during amino acid starvation. *Nat. Commun.* **8**, 338
  55. Scherz-Shouval, R., and Elazar, Z. (2011) Regulation of autophagy by ROS: Physiology and pathology. *Trends Biochem. Sci.* **36**, 30–38
  56. Zhou, J., Li, X. Y., Liu, Y. J., Feng, J., Wu, Y., Shen, H. M., and Lu, G. D. (2021) Full-coverage regulations of autophagy by ROS: From induction to maturation. *Autophagy*. <https://doi.org/10.1080/15548627.2021.1984656>
  57. Ding, W. X., and Yin, X. M. (2012) Mitophagy: Mechanisms, pathophysiological roles, and analysis. *Biol. Chem.* **393**, 547–564
  58. Flem-Karlsen, K., Fodstad, O., Tan, M., and Nunes-Xavier, C. E. (2018) B7-H3 in cancer - beyond immune regulation. *Trends Cancer* **4**, 401–404
  59. Liu, B., Sun, L., Liu, Q., Gong, C., Yao, Y., Lv, X., Lin, L., Yao, H., Su, F., Li, D., Zeng, M., and Song, E. (2015) A cytoplasmic NF-kappaB interacting long noncoding RNA blocks IkappaB phosphorylation and suppresses breast cancer metastasis. *Cancer Cell* **27**, 370–381
  60. Emens, L. A., Molinero, L., Loi, S., Rugo, H. S., Schneeweiss, A., Dieras, V., Iwata, H., Barrios, C. H., Nechaeva, M., Nguyen-Duc, A., Chui, S. Y., Husain, A., Winer, E. P., Adams, S., and Schmid, P. (2021) Atezolizumab and nab-paclitaxel in advanced triple-negative breast cancer: Biomarker evaluation of the IMpassion130 study. *J. Natl. Cancer Inst.* **113**, 1005–1016
  61. Su, S., Liu, Q., Chen, J., Chen, J., Chen, F., He, C., Huang, D., Wu, W., Lin, L., Huang, W., Zhang, J., Cui, X., Zheng, F., Li, H., Yao, H., *et al.* (2014) A positive feedback loop between mesenchymal-like cancer cells and macrophages is essential to breast cancer metastasis. *Cancer Cell* **25**, 605–620
  62. Huang, D., Chen, J., Yang, L., Ouyang, Q., Li, J., Lao, L., Zhao, J., Liu, J., Lu, Y., Xing, Y., Chen, F., Su, F., Yao, H., Liu, Q., Su, S., *et al.* (2018) NKILA lncRNA promotes tumor immune evasion by sensitizing T cells to activation-induced cell death. *Nat. Immunol.* **19**, 1112–1125